scientific reports

OPEN

Multiple Walker breakdowns in magnetic multilayers

Joon Moon[1,3], Jaesung Yoon[1,3], Kitae Kim[1], Seong-Hyub Lee[1], Dae-Yun Kim[2] & Sug-Bong Choe[1✉]

Herein, we report an exotic domain-wall dynamics showing double Walker breakdowns in magnetic multilayer films composed of two magnetic layers. Such multiple Walker breakdowns are attributed to the internal magnetic dipole field, which is antisymmetric on the domain walls of the lower and upper magnetic layers. A micromagnetic simulation shows four phases of the domain-wall dynamics, which result in a phase diagram with the phase boundaries of the double Walker breakdown fields. Such double Walker breakdowns lead to two minima in the variation of the domain-wall velocity, as often observed experimentally.

Recently, magnetic thin films have drawn great technological attention because of their prospects for use in next-generation memory and logic devices[1,2]. The data bits in these devices are stored in their magnetization states and/or ordering structures such as magnetic domains and domain walls (DWs). The device operation is therefore performed by switching between the magnetization states as done for the magnetic random-access memory and/or the displacement of magnetic structures as done for the magnetic racetrack memory[3,4]. These magnetization dynamics and their characteristics are determined by magnetic parameters such as perpendicular magnetic anisotropy, Dzyaloshinskii–Moriya interaction, and the spin–orbit coupling effect[5–9]. As these phenomena are generated at interfaces adjacent to magnetic layers, much effort has been devoted to controlling the interface properties in magnetic thin films and multilayered structures[10].

For multilayered structures with multiple magnetic layers, the magnetic properties of each magnetic layer are largely determined by their own interfaces. Because ensuring the homogeneity among all interfaces is difficult, it is natural that each magnetic layer has magnetic properties different from the others[11,12]. Static magnetic properties, such as the stable DW configuration, have been reported to significantly affect the dynamics of the DW motion[13]. For example, a stable DW configuration determines the direction of DW motion driven by the spin–orbit torque. Therefore, it is essential to understand the layer resolved DW configurations and their roles in DW dynamics in magnetic multilayered structures.

Most of the studies of magnetic DW motion in magnetic multilayered structures was done without consideration of the DW configuration. Only a few studies have focused on the DW configurations in magnetic multilayered structures[14,15]. Since the magnetic DW motion in magnetic multilayered structures have drawn more attention in magnetic application devices[1–4], more comprehensive understanding on the magnetic DW motion is required within the context of the DW configuration.

In this study, we prepared magnetic multilayered structures composed of two magnetic layers and then investigated the DW dynamics in these structures using a magneto-optical Kerr effect microscope. Interestingly, the magnetic multilayered structures exhibit an exotic coupled behavior of the DW dynamics. A micromagnetic study was carried out to explain the exotic coupled behavior within the context of multiple Walker breakdowns of DWs in each magnetic layer.

Results

Double minimum of DW velocity about H_x. The DW displacements are measured along the direction (Fig. 5d, yellow arrow) parallel to H_x, providing the DW speed, v_{DW}, in the direction of H_x. Figure 1a,b plot the measured v_{DW} onto the 2-dimensional (2D) coordinate plane with respect to H_x (abscissa) and H_z (ordinate) for Samples I and II, respectively. Sample I exhibits a typical symmetrical v_{DW} variation with respect to H_x. The line profile along the dashed red line in Fig. 1a is plotted in Fig. 1c, clearly confirming the symmetrical variation with a single minimum. Such symmetrical variation is known to be caused by the evolution of the stable DW configuration under the influence of H_x[13].

[1]Department of Physics and Astronomy, Seoul National University, Seoul 08826, Republic of Korea. [2]Department of Electrical and Computer Engineering, National University of Singapore, Singapore 117582, Singapore. [3]These authors contributed equally: Joon Moon and Jaesung Yoon. ✉email: sugbong@snu.ac.kr
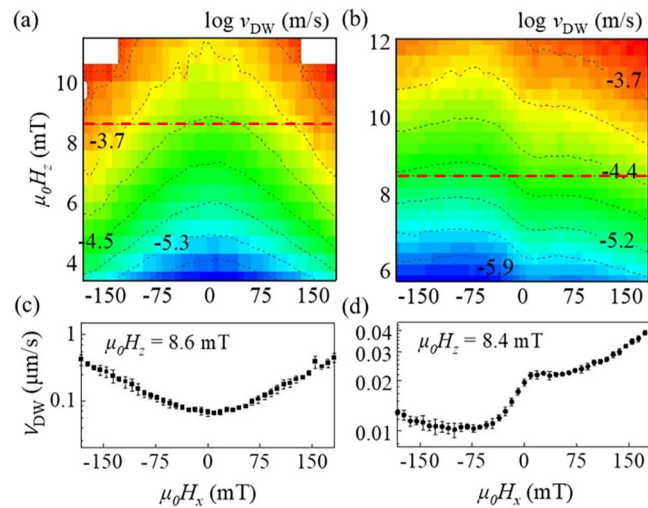
Figure 1. (**a,b**) 2-dimensional plots of log v_{DW} with respect to H_x (abscissa) and H_z (ordinate) for Samples I and II, respectively. (**c,d**) Line profiles of v_{DW} with respect to H_x along the horizontal lines in (**a**) and (**b**), respectively.
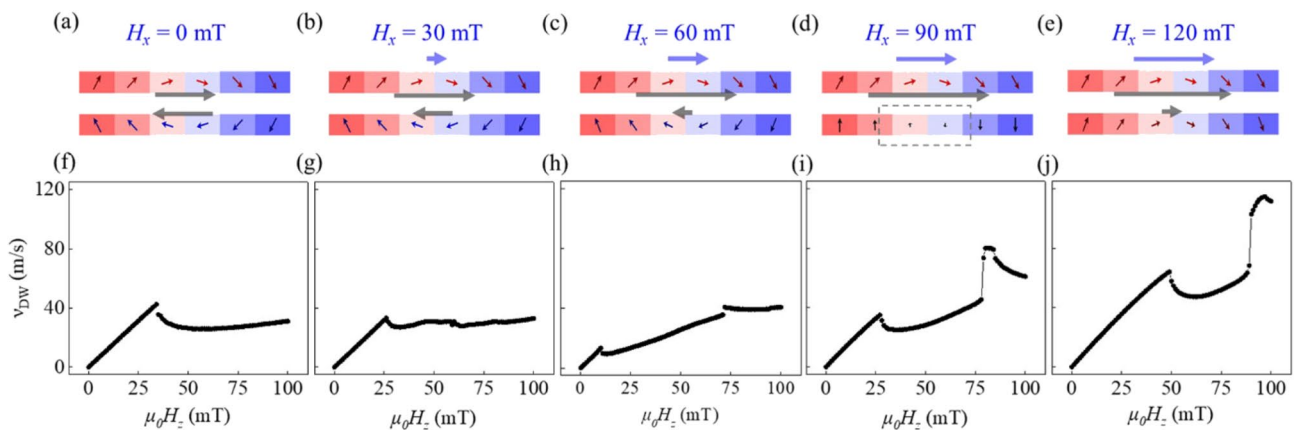

Figure 2. DW configurations under various H_x values of (**a**) 0 mT, (**b**) 30 mT, (**c**) 60 mT, (**d**) 90 mT, and (**e**) 120 mT. The arrow inside each mesh shows the direction of the magnetization. The colors of arrows and meshes correspond to the x and z components of the magnetization, respectively. The gray arrows show H_{tot} at the upper and lower magnetic layer. The blue arrow shows the strength of H_x. (**f–j**) Plots of v_{DW} with respect to H_z for different H_x values.

Interestingly, Sample II shows an exotic variation of v_{DW} with two minima, as shown in the 2D plot of Fig. 1b and the line profile in Fig. 1d. Though it is well known that the asymmetry of v_{DW} near $H_x \cong 0$ is ascribed to the Dzyaloshinskii–Moriya interaction[13,16], the exotic variation with two minima goes well beyond the model based on a single DW configuration. To check whether the exotic variation with two minima is ascribed to the two magnetic layers as in Sample II, the coupled configuration between the DWs in the two magnetic layers was investigated by considering micromagnetism. The simulation results are discussed hereafter.

Multiple walker breakdown. The stationary DW configurations at $H_z = 0$ were first examined under application of H_x over the range from 0 to 120 mT. Figure 2a–e shows the cross-sectional view of the stable DW configurations in the stationary state for different H_x values of (a) 0, (b) 30, (c) 60, (d) 90, and (e) 120 mT, respectively. The arrow inside each mesh shows the direction of the magnetization. The color of each arrow corresponds to the x component of the magnetization (red for $+x$ direction and blue for $-x$ direction), whereas the color inside each mesh corresponds to the z component of the magnetization (red for $+z$ direction and blue for $-z$ direction).

When $H_x = 0$, as shown in Fig. 2a, the dipolar magnetic field from the lower magnetic layer generates a local magnetic field, H_{dip}. For the present geometry, such H_{dip} has a net in-plane component along the $+x$ direction (upper gray arrow) at the position of the DW in the upper magnetic layer. Thus, the upper DW becomes stabilized as the Néel-type configuration with internal magnetization along the $+x$ direction. Inversely, the dipolar magnetic
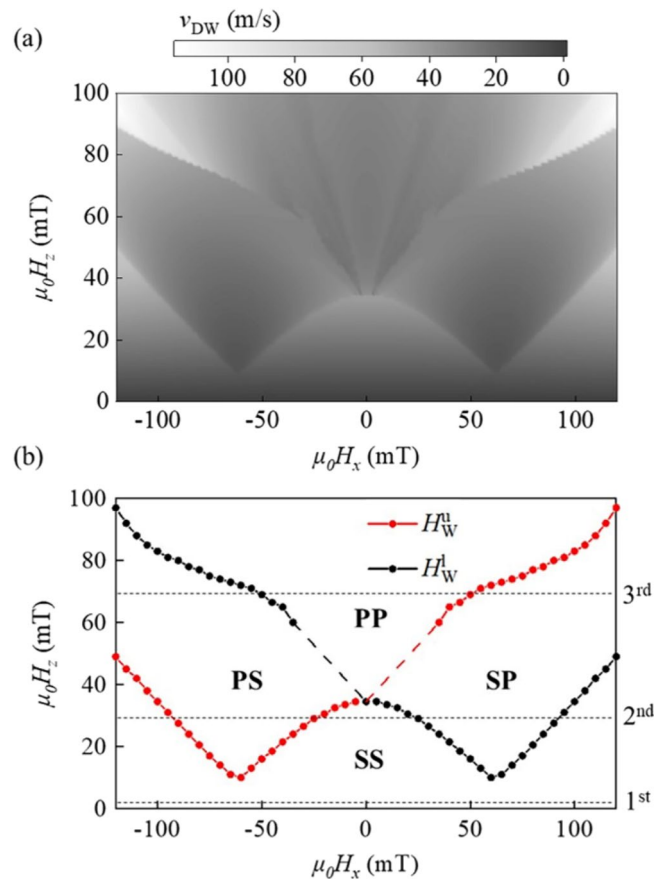
Figure 3. (**a**) 2-dimensional plots of the calculated v_{DW} with respect to H_x (abscissa) and H_z (ordinate). (**b**) Phase diagram of the PP, PS, SP, and SS phases. The red and black lines indicate the Walker breakdown fields, H_W^u and H_W^l, of the upper and lower layers, respectively. The horizontal lines are the paths of the line profiles shown in Fig. 4.

field from the upper magnetic layer generates a net H_{dip} along the $-x$ direction (lower gray arrow) at the lower DW, thus resulting in the opposite Néel-type configuration along the $-x$ direction. Consequently, an antiparallel alignment of the internal magnetization appears between the upper and lower DWs, as shown in Fig. 2a.

Under the application of H_x (blue arrows), the total in-plane magnetic field, H_{tot} ($= H_x + H_{dip}$) becomes unbalanced at positions between the upper and lower DWs. For the present geometry, an increase in H_x causes the decrease of H_{tot} at the lower DW, as shown by the lower gray arrows in Fig. 2b,c. When H_{tot} vanishes, the DW becomes a Bloch-type configuration, as shown in Fig. 2d. A further increase in H_x results in the parallel alignment of the internal magnetization between the upper and lower DWs, as shown in Fig. 2e.

To examine the effect of these different DW configurations, the DW speed, v_{DW} is calculated under the application of H_z. Figure 2f–j plot v_{DW} with respect to H_z for different H_x values. When $H_x = 0$, as shown in Fig. 2f, v_{DW} exhibits an abrupt breakdown at a certain strength of H_z. This breakdown is well known as the Walker breakdown, which is caused by the precession of the internal magnetization inside the DWs.

Phases of DW during DW motion. Figure 3a shows a 2D plot of v_{DW} with respect to H_x (abscissa) and H_z (ordinate). It is clear from the plot of several different phases with phase boundaries. The phase boundaries are attributed to the Walker breakdown, below which a steady-state motion with a fixed magnetization angle appears, above which a precessional motion occurs. For better visualization, Fig. 3b illustrates the four phases: phase SS of steady-state motions (both DWs), phase PS of precessional (upper DW) and steady-state (lower DW) motions, phase SP of steady-state (upper DW) and precessional (lower DW) motions, and phase PP of precessional motions (both DWs). The phase boundaries indicate the Walker breakdown fields, H_W^u (red symbols) and H_W^l (black symbols), for the upper and lower DWs, respectively.

Inside the phase diagram, the line profiles (horizontal dashed lines) under a fixed H_z provide the v_{DW} variation with respect to H_x, similar to the experimental measurement procedure, shown in Fig. 1d.

DW velocity by walker breakdown. Figure 4a–c plot the v_{DW} variation with respect to H_x under several fixed H_z values. Here, the presents v_{DW} variations can be considered as the global v_{DW} of the bilayer (as seen in Fig. 2) and then, be explained by the combined effect of the DWs of the lower and upper layers (as seen in
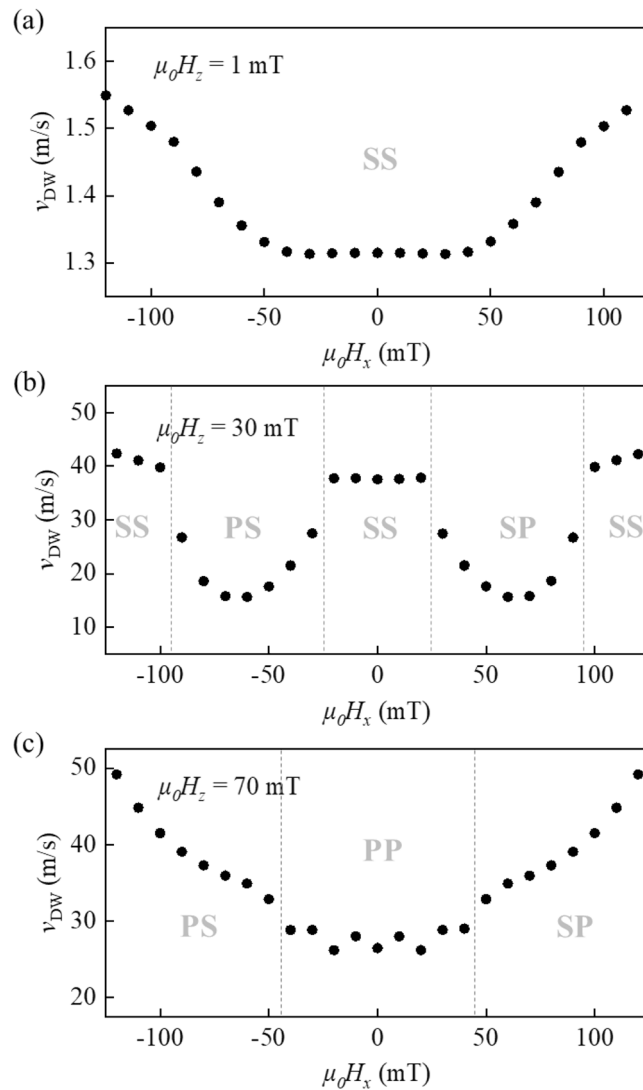
Figure 4. Line profiles of v_{DW} with respect to H_x under fixed H_z of (**a**) 1, (**b**) 30, and (**c**) 70 mT. The paths of the line profiles are shown by the horizontal lines in Fig. 3b.

Fig. 3). For a weak H_z, the line profile along the first horizontal dashed line in Fig. 3b stays inside phase SS for both DWs. The v_{DW} variation almost exhibits a plateau in the middle with respect to H_x, as shown in Fig. 4a. However, a closer observation showed two separated minima with small amplitudes. These separated minima become obvious for an intermediate H_z, where the line profile along the second horizontal, dashed line in Fig. 3b crosses phases PS, SS, and SP. Because v_{DW} in phases PS and SP is largely reduced owing to the Walker breakdown, the v_{DW} variation naturally exhibits two large minima inside these phases, as shown in Fig. 4b. Finally, for a strong H_z, the line profiles along the third horizontal dashed line in Fig. 3b cross phases PS, PP, and SP. Because the v_{DW} of phase PP is slower than those of the other phases owing to the Walker breakdowns for both DWs, its v_{DW} variation exhibits a single minimum at the middle, that is, inside phase PP, as shown in Fig. 4c. Notably, the experimental value of H_z in Fig. 1b ranges between those values shown in Fig. 4a,b. Therefore, the double Walker breakdowns for each DW of the two magnetic layers can explain the experimental observation of the exotic v_{DW} variation.

Discussion

The magnetic field for the breakdown is denoted as the Walker breakdown field, H_W. According to Ref.[17], H_W follows the relation, $H_W = \alpha \sin \psi_W (|H_{tot}| - H_{DW} \cos \psi_W)$, where H_{DW} is the DW anisotropy field. Here, azimuthal angle ψ_W of the magnetization inside the DW is defined as $\cos \psi_W = \left(|H_{tot}| - \sqrt{H_{tot}^2 + 8H_{DW}^2} \right) / 4H_{DW}$.

In addition, when $H_x = 0$, both the upper and lower DWs have the same $|H_{tot}|$ value, resulting in identical strengths of H_W. Therefore, both DWs exhibit a single Walker breakdown simultaneously, as shown in Fig. 2f. However, under the application of H_x, the upper and lower DWs have different values of $|H_{tot}|$, resulting in
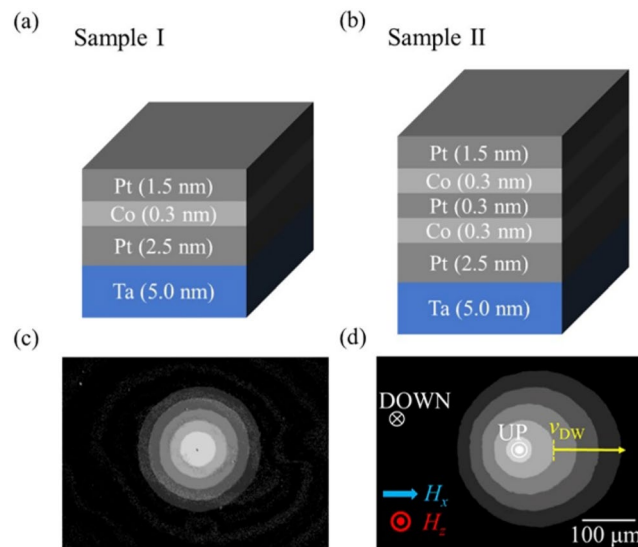
Figure 5. (**a,b**) Layer structures of Samples I and II, respectively. (**c,d**) Magnetic domain expansion images overlaid with the snapshots taken at a specified time interval for Samples I and II, respectively. The blue arrow and red symbol represent directions of H_x and H_z, respectively. The white symbols indicate the directions of magnetization. The brightest circle in the middle represents the initial magnetic domain. The yellow arrow indicates the direction of the v_{DW} measurement.

different strengths of H_W. This could possibly result in two separate Walker breakdowns. As H_x increases, such a separation becomes more obvious and dominant, as shown in Fig. 2g–j.

In summary, we investigated the phases of the DW motion among two magnetic layers. The micromagnetic simulation results reveal that each magnetic layer has a different internal dipolar magnetic field, and thus the DW in each magnetic layer experiences different magnetic fields. Owing to the different Walker breakdown fields for each DW, the v_{DW} variation exhibits two minima with respect to H_x. The presented simulation results satisfactorily explain the experimental observation of the two minima in the v_{DW} variation.

Methods

Sample preparations and DW velocity measurements.
For this study, we prepared two types of magnetic films with different numbers of magnetic layers. Here, we denote Samples I and II for films composed of a single magnetic layer and double magnetic layers, respectively. The detailed layered structures comprise 5-nm Ta/2.5-nm Pt/0.3-nm Co/1.5-nm Pt for Sample I and 5-nm Ta/2.5-nm Pt/0.3-nm Co/0.3-nm Pt/0.3-nm Co/1.5-nm Pt for Sample II, as illustrated in Fig. 5a,b, respectively. The films were deposited on Si wafers with a 100-nm SiO$_2$ layer using dc magnetron sputtering.

Both films exhibited strong perpendicular magnetic anisotropy and clear magnetic domain patterns. Figure 5c,d shows the magnetic domain images of Samples I and II, respectively. Each image is overlaid with several snapshots taken by magneto-optical Kerr effect (MOKE) microscopy at a specified time interval under the application of the out-of-plane magnetic field, H_z (red symbol), together with the in-plane magnetic field, H_x (blue arrow)[13]. The brightest circle in the middle represents the initial circular magnetic domain, which exhibits gradual expansion over time, as shown by the gradual change in image contrast.

Micromagnetic simulation.
We employed the object-oriented micromagnetic framework (oommf) code in three-dimensional geometry. The simulation geometry was set as a lateral wire structure onto the film of two ferromagnetic (FM) layers separated by a nonmagnetic (NM) spacer. The lateral wire structure has a length of 2000 nm and a width of 250 nm. All FM and NM layers have an identical thickness of 0.4 nm. The mesh size was chosen to be 1 nm along the length, 250 nm along the width, and 0.4 nm along the thickness. For a fast simulation speed with minimal number of meshes, the mesh size along the width is set to be identical to the wire width. The mesh size along the length was set to be sufficiently small to describe the internal DW structures. The magnetic parameters are chosen as the typical values of Co/Pt multilayers, as given by the exchange stiffness of 5×10^{-12} J/m, saturation magnetization of 1.4×10^6 A/m, and surface magnetic anisotropy of 1.93×10^6 J/m^3[18]. For fast relaxation to the ground state, the damping constant was set at $\alpha = 0.5$.

Data availability

The datasets generated during and/or analysed during the current study are available from the corresponding author on reasonable request.

References

1. Chappert, C., Fert, A. & Van Dau, F. N. The emergence of spin electronics in data storage. *Nat. Mater.* **6**, 147–157 (2007).
2. Luo, Z. *et al.* Current-driven magnetic domain-wall logic. *Nature* **579**, 214–218 (2020).
3. Daughton, J. M. Magnetic tunneling applied to memory (invited). *J. Appl. Phys.* **81**, 3758 (1997).
4. Parkin, S. S. P., Hayashi, M. & Thomas, L. Magnetic domain-wall racetrack memory. *Science* **320**, 190–194 (2008).
5. Bellec, A., Rohart, S., Labrune, M., Miltat, J. & Thiaville, A. Domain wall structure in magnetic bilayers with perpendicular anisotropy. *Europhys. Lett.* **91**, 17009 (2010).
6. Haazen, P. P. J. *et al.* Domain wall depinning governed by the spin Hall effect. *Nat. Mater.* **12**, 299–303 (2013).
7. Miron, I. M. *et al.* Perpendicular switching of a single ferromagnetic layer induced by in-plane current injection. *Nature* **476**, 189–193 (2011).
8. Liu, L. *et al.* Spin-torque switching with the giant spin Hall effect of tantalum. *Science* **336**, 555–558 (2012).
9. Emori, S., Bauer, U., Ahn, S. M., Martinez, E. & Beach, G. S. D. Current-driven dynamics of chiral ferromagnetic domain walls. *Nat. Mater.* **12**, 611–616 (2013).
10. Park, Y. K. *et al.* Interfacial atomic layers for full emergence of interfacial Dzyaloshinskii–Moriya interaction. *NPG Asia Mater.* **12**, 38 (2020).
11. Hrabec, A. *et al.* Velocity enhancement by synchronization of magnetic domain walls. *Phys. Rev. Lett.* **120**, 227204 (2018).
12. Lemesh, I. & Beach, G. S. D. Walker breakdown with a twist: Dynamics of multilayer domain walls and skyrmions driven by spin-orbit torque. *Phys. Rev. Appl.* **12**, 044031 (2019).
13. Je, S. G. *et al.* Asymmetric magnetic domain-wall motion by the Dzyaloshinskii–Moriya interaction. *Phys. Rev. B* **88**, 214401 (2013).
14. Purnama, I., Kerk, I. S., Lim, G. J. & Lew, W. S. Coupled Néel domain wall motion in sandwiched perpendicular magnetic anisotropy nanowires. *Sci. Rep.* **5**, 8754 (2015).
15. Metaxas, P. J. *Domain Wall Dynamics in Ultrathin Ferromagnetic Film Structures: Disorder, Coupling and Periodic Pinning* (The University of Western Australia, 2009).
16. Moon, K.-W. *et al.* Magnetic bubblecade memory based on chiral domain walls. *Sci. Rep.* **5**, 9166 (2015).
17. Thiaville, A., Rohart, S., Jué, É., Cros, V. & Fert, A. Dynamics of Dzyaloshinskii domain walls in ultrathin magnetic films. *Europhys. Lett.* **100**, 57002 (2012).
18. Donahue, M. J. & Porter, D. G. *OOMMF User's Guide, Version 1.0. Interagency Report NISTIR 6376* (National Institute of Standards and Technology, 1999).

Acknowledgements

Author contributions

J.M. and D.-Y.K. designed this study. J.M. and S.-H.L. fabricated samples. J.M. and K.K. performed experiments. J.M. and J.Y. performed simulations. J.M., J.Y. and S.-B.C analyzed the data and wrote the manuscript. All authors discussed the results and commented on the manuscript. J.M. and J.Y. contributed equally to this work.

Competing interests

The authors declare no competing interests.

Additional information

Correspondence and requests for materials should be addressed to S.-B.C.

Reprints and permissions information is available at www.nature.com/reprints.

Publisher's note Springer Nature remains neutral with regard to jurisdictional claims in published maps and institutional affiliations.